Influence of nonequilibrium lipid transport, membrane compartmentalization, and membrane proteins on the lateral organization of the plasma membrane

Jun Fan and Maria Sammalkorpi
Department of Mechanical and Aerospace Engineering, Princeton University, Princeton, New Jersey 08544, USA

Mikko Haataja
Department of Mechanical and Aerospace Engineering, Princeton Institute for the Science and Technology of Materials (PRISM) and Program in Applied and Computational Mathematics (PACM), Princeton University, Princeton, New Jersey 08544, USA

(Received 26 March 2009; revised manuscript received 16 September 2009; published 14 January 2010)

Compositional lipid domains (lipid rafts) in plasma membranes are believed to be important components of many cellular processes. The mechanisms by which cells regulate the sizes, lifetimes, and spatial localization of these domains are rather poorly understood at the moment. We propose a robust mechanism for the formation of finite-sized lipid raft domains in plasma membranes, the competition between phase separation in an immiscible lipid system and active cellular lipid transport processes naturally leads to the formation of such domains. Simulations of a continuum model reveal that the raft size distribution is broad and the average raft size is strongly dependent on the rates of cellular and interlayer lipid transport processes. We demonstrate that spatiotemporal variations in the recycling may enable the cell to localize larger raft aggregates at specific parts along the membrane. Moreover, we show that membrane compartmentalization may further facilitate spatial localization of the raft domains. Finally, we demonstrate that local interactions with immobile membrane proteins can spatially localize the rafts and lead to further clustering.

DOI: 10.1103/PhysRevE.81.011908 PACS number(s): 87.14.Cc, 87.15.A−, 87.16.D−

I. INTRODUCTION

The plasma membrane is a bilayer composed primarily of thousands of types of lipids and membrane proteins. It functions as the physical boundary of cells, as well as a selective sieve through which matter and information are exchanged between cells and their environment. To describe the membrane "microstructure," i.e., the spatial variations in the local lipid compositions and proteins, Singer and Nicolson initially proposed that membranes are two-dimensional spatially homogeneous mixtures of lipids and proteins [1]. However, many subsequent experimental findings supported a rather different picture, namely that membranes are highly heterogeneous [2–5], consisting of a mixture of a "liquid ordered" (l_o) phase [6], often called "lipid rafts" [7], and a "liquid disordered" (l_d) phase. The lipid rafts consist mainly of cholesterol and saturated lipids, such as sphingolipids. Lipid rafts have been implicated in processes such as signal transduction [7–10], membrane trafficking [7,11–13], and protein sorting [8,14]. Additionally, virus entry, assembly, and budding are also facilitated by the raft domains [15–17]. A comprehensive review of experimental methods employed in raft research can be found in [18].

Although lipid rafts have not been directly observed *in vivo*, there exists compelling indirect evidence to support their existence [19–27]. The consensus is that the rafts *in vivo* are highly dynamic dispersed microdomains [19] of size $20\sim200$ nm [20–25], with life times ranging from $\sim10^{-2}$ s to $\sim10^{3}$ s [20,23–25]. The area fraction of the microdomains is estimated to be $10\%\sim15\%$ [23,26] and they contain perhaps $10\sim100$ proteins per domain [21,23,28]. These raft proteins may be connected to the cytoskeleton [29], and the spatial distribution of the microdomains may depend on their coupling to the cytoskeleton [25,29]. In contrast to *in vivo* membranes, phase separation and l_o/l_d phase coexistence have been observed in model membranes, such as monolayers [30,31], bilayers on supported substrate [32], and giant unilamellar vesicles (GUVs) [30,33–35]. Most notably, in model membranes the raft domain size is ~1 μm, comparable to the system size.

The fundamental questions is, therefore, why are there large, persistent l_o domains present in model membranes but not in living cells? One crucial difference between the two systems is that in comparison to living cell membranes, model membranes do not have cellular processes, such as vesicle trafficking [36,37] or fast lipid flip-flopping between two leaflets [38,39] assisted by translocases [40,41], which are critical in maintaining the asymmetric lipid distribution across the bilayer [42]. Furthermore, model membranes do not contain proteins or cytoskeleton, nor the resulting molecular interactions. As we will argue later in this paper, the aforementioned cellular processes can play a critical role in the regulation of raft domains.

Theoretical models developed to explain the raft formation mechanism generally fall into two categories—those invoking thermodynamic equilibrium and those allowing for nonequilibrium effects. An example of the former is the model by Yethiraj and Weisshaar [43], similar to the quenched-disorder random bond Ising model [44], in which immobile proteins reside in an immiscible lipid system and the critical temperature is found to be lower than that of the pure immiscible lipid system [43]. The proteins act as surfactants and may stabilize compositional microdomains, which would explain why larger raft domains have not been observed *in vivo*. However, if one allows the membrane proteins to diffuse, the critical temperature would be suppressed to a lesser degree as in the case of the annealed-disorder random bond Ising model [45,46], indicating that macro-

scopic phase separation may still occur at the body temperature. In [47], both lipid phase separation and a coupling to a lipid reservoir were introduced. Phase separation by itself would give rise to domain coarsening while coupling to the reservoir suppresses domain growth. In this model, it is assumed that lipid transport between the membrane and the reservoir is proportional to the local lipid density, which results in a steady state with a distribution of roughly equal-sized domains. Although the model was framed as a nonequilibrium one, it is interesting to note that it reduces to an effective equilibrium model for a block copolymer [48], and the raft size can be identified with the effective block size in thermal equilibrium. It has also been suggested very recently that the body temperature is slightly above a critical temperature, and the raft domains are simply manifestations of critical compositional fluctuations [49].

Existing models based on nonequilibrium effects [50–54], on the other hand, argue that raft formation and regulation require cellular activity via facilitated lipid transport to and from the membrane (lipid recycling). In [50], the stochastic addition or removal of lipid domains to or from the membrane results in a broad domain size distribution. A very similar model to the one in [47] was recently introduced by Gómez *et al.* [53,54]. In this model, the evolution of a ternary system (cholesterol, saturated lipid, and unsaturated lipid) was studied in the presence of a coupling to a cholesterol reservoir. This coupling induces a spatially patterned cholesterol distribution, leading to the suppression of macroscopic phase separation. In contrast to the domains observed in [50,52], the raft domains in this case have a rather uniform size distribution and appear circular. Reference [51], on the other hand, describes a single lipid species nonequilibrium model without phase separation. In this model, vesicular trafficking brings patches of lipids to the membrane, while diffusion barriers due to membrane compartmentalization lead to transient spatial localization of the patches. Finally, very recently we proposed a nonequilibrium model, in which phase separation driven domain coarsening and recycling due to vesicular and nonvesicular lipid trafficking events compete. This competition results in a broad raft domain size distribution, whose properties are dictated by the rate and spatial extent of recycling [52]. A very recent review on the theoretical models for raft formation can be found in [55].

From the discussion above, it should be clear that lipid raft formation is a complex process, in which various factors may play a role. In this paper, we continue our previous efforts of [52] and extend the model to include the combined effects of phase separation, lipid trafficking, membrane proteins, and diffusion barriers on the raft formation process. Overall, we find that the key process that maintains a finite domain distribution is rapid lipid trafficking, which counteracts domain coarsening driven by line tension between the compositional domains. We also demonstrate that spatiotemporal variations in the recycling may enable the cell to localize larger raft aggregates at specific parts along the membrane. Other processes such as membrane and cytoskeleton interactions, as well as membrane protein and lipid interactions can also regulate the size and spatial distribution of the raft domains.

The rest of this paper is organized as follows: the theoretical model is formulated in Sec. II, and analytical arguments for the appearance and properties of raft domains are given. Results from numerical simulations of the model are then presented in Sec. III. In particular, the effects of phase separation, lipid trafficking, diffusion barriers, and immobile membrane proteins on the raft formation process are explored. Finally, a discussion can be found in Sec. IV, while the Appendix contains some of the more detailed analytical derivations.

II. MODEL

Standard approaches to investigate multicomponent lipid bilayer systems computationally include atomistic molecular dynamics (MD) [56–59], dissipative particle dynamics (DPD) [60–65], and phenomenological continuum "phase-field" simulations [66–71]. As both the MD and DPD methods are rather restricted in terms of particle numbers and time scales, they are not well suited for studying collective phenomena involving cellular processes; therefore, a continuum approach will be developed.

A. Synthetic membranes: thermodynamics and kinetics

The plasma membrane contains thousands of types of lipids, which can be classified into three categories: steroids, saturated lipids, and unsaturated lipids. Therefore, a physically based model of the plasma membrane should at least contain one species from each category. A well-characterized example of such a system is a mixture of cholesterol, dipalmitoylphosphatidylcholine (DPPC), and diolephosphatidylcholine (DOPC). Veatch and Keller have characterized successfully GUVs consisting of cholesterol, DPPC, and DOPC, and observed domain coarsening of the l_o and l_d phases [30,34]. To explain these experimental observations, Radhakrishnan and McConnell proposed a thermodynamic model wherein cholesterol and DPPC form a complex, which then subsequently phase separates from DOPC [72]. As a result, l_o and l_d phase separation occurs within certain composition regimes of the mixture of cholesterol, DPPC, and DOPC in GUVs below the critical temperature.

1. Thermodynamics

Based on this ternary system, a continuum model may be developed as follows. The free energy of a mixture of cholesterol, DOPC, DPPC, and cholesterol-DPPC complex written in terms of mole fractions x_i becomes

$$f = \sum_i x_i(G_i + k_B T \ln x_i) + 2k_B T_c x_{US} x_{CX}, \tag{1}$$

where k_B is the Boltzmann constant, G_i is the free energy of each pure component, $x_i \ln x_i$, represents the entropy of mixing, while $2k_B T_c x_{US} x_{CX}$ is the enthalpy of mixing of the unsaturated lipid (DOPC) and the complex (cholesterol-DPPC). The enthalpy of mixing is assumed negligible for the other pairs since they are miscible. T_c denotes the critical temperature of phase separation. Furthermore, to simplify the derivation, we assume below that complex formation between cholesterol and DPPC is complete, and that initially cholesterol and DPPC are present in equal proportions. In this case,

the system can be described as a two component system composed of the cholesterol-DPPC complex and the unsaturated lipid (DOPC). Equation (1), thus, becomes

$$f = k_B T(x_{US} \ln x_{US} + x_{CX} \ln x_{CX}) + 2k_B T_c x_{US} x_{CX}, \quad (2)$$

where $x_{US}G_{US}+x_{CX}G_{CX}$ is taken as a constant and hence dropped from the subsequent analysis. Furthermore, by replacing x_{CX} with $(1-c)/2$ and x_{US} with $(1+c)/2$, Eq. (2) becomes

$$f(c,T) = \frac{k_B T}{2}\left[(1+c)\ln\frac{1+c}{2} + (1-c)\ln\frac{1-c}{2}\right] + k_B T_c(1-c^2)/2. \quad (3)$$

In the limit $c \to 0$, that is, close to the critical point, Eq. (3) takes the form,

$$f(c) = -\frac{u}{2}c^2 + \frac{v}{4}c^4, \quad (4)$$

where $u=k_B(T_c-T)$, $v=k_BT/3$, and unimportant constant terms have been ignored. Finally, to account for spatial heterogeneities in the local compositions, the total free energy of the system is written,

$$F = \int_{\mathbf{r}} \left(-\frac{u}{2}c^2 + \frac{v}{4}c^4 + \frac{\kappa}{2}(\nabla c)^2\right) d\mathbf{r}, \quad (5)$$

where κ denotes the so-called gradient energy coefficient [73] and is related to the line tension between phases of varying compositions.

As discussed in [72], allowing for incomplete complex formation and unequal amounts of cholesterol and DPPC does not change the qualitative picture that emerges, namely, that of a ternary system with a substantial miscibility gap and two-phase coexistence. Within the miscibility gap, the mixture is effectively a two-phase system, and the above considerations apply with a suitable redefinition of c as the order parameter distinguishing between the co-existing phases.

2. Kinetics

Given the free energy functional of the system, the relaxational dynamics of the c field in the vicinity of the critical point can be written as [74],

$$\frac{\partial c(\mathbf{r},t)}{\partial t} = -\nabla\cdot\vec{j} + \epsilon(\mathbf{r},t) = \nabla\cdot\left[M\,\nabla\,\frac{\delta F}{\delta c}\right] + \epsilon(\mathbf{r},t) = \nabla\cdot[M\,\nabla\,(-uc + vc^3 - \kappa\nabla^2 c)] + \epsilon(\mathbf{r},t), \quad (6)$$

where M is the mobility (assumed isotropic in this work), and ϵ denotes a stochastic Gaussian noise with mean $\langle\epsilon\rangle=0$ and variance $\langle\epsilon(\mathbf{r}_1,t_1)\epsilon(\mathbf{r}_2,t_2)\rangle=-2Mk_BT\nabla^2\delta(\mathbf{r}_1-\mathbf{r}_2)\delta(t_1-t_2)$ as dictated by the fluctuation-dissipation theorem.

The dimensionless form of the above equation of motion (model B in the classification of Hohenberg and Halperin [74]) can be written,

$$\frac{\partial c'}{\partial \tau} = \nabla'\cdot[M'\nabla'(-c' + c'^3 - \nabla'^2 c')] + \epsilon'(\mathbf{r}',\tau). \quad (7)$$

The dimensionless quantities are related to their dimensionless counterparts via $c=\sqrt{\frac{u}{v}}c'$, $\mathbf{r}=\sqrt{\frac{\kappa}{u}}\mathbf{r}'$, and $t=\frac{\kappa}{M_{\max}u^2}\tau$. The dimensionless noise correlator obeys $\langle\epsilon'(\mathbf{r}_1',\tau_1)\epsilon'(\mathbf{r}_2',\tau_2)\rangle = -\frac{2k_BTv}{u\kappa}\nabla'^2\delta(\mathbf{r}_1'-\mathbf{r}_2')\delta(\tau_1-\tau_2)$, and the dimensionless mobility $M'\equiv M/M_{\max}$, where $M_{\max}$ denotes the maximum value of M. In the following, we will continue working with the dimensionless quantities but drop the primes for notational clarity. In Eq. (7), space and time are measured in the units of the mean-field correlation length and characteristic relaxation time of the system, respectively, both of which diverge as the critical point is approached. Furthermore, $c=-1$ represents the l_o raft phase, while $c=1$ represents the l_d phase.

The physics of Eq. (7) are well known and have been studied by many authors [73,75–77], both in the presence and absence of thermal fluctuations. The binary system equilibrates via a phase separation, in which the l_d and l_o domains continually coarsen to reduce the excess interfacial energy, as long as the magnitude of thermal fluctuations is below a threshold value. For large enough thermal fluctuations, on the other hand, the system is effectively above its critical point and does not phase separate. Models of this kind have been employed in the past to investigate both the phase behavior and phase separation dynamics in spherical GUVs [66–68] and other geometries [69–71], with additional coupling terms to describe the local curvature or deformation of the membrane.

B. Plasma membranes: nonequilibrium effects

Although very convenient and well-characterized, model membrane systems do not incorporate many of the essential features of real plasma membranes, including lipid trafficking to and from the membrane. For an improved model of the plasma membrane, we next incorporate lipid transport processes and local protein/cytoskeleton interactions to the above model describing a model membrane [i.e., Eq. (7)].

With regard to active lipid transport processes, our main assumption is that due to active vesicular trafficking events [50–54], lipids are transported to and from the plasma membrane randomly in time and space such that the overall average composition of the membrane remains unchanged, as illustrated schematically in Fig. 1. In addition, various protein activity, for example, scramblase, flippase and floppase proteins [40,41] shuffle lipids between the plasma membrane leaflets. Instead of modeling each individual event, we attempt to incorporate the net effect of all these stochastic processes in a phenomenological manner.

This part of the theory may be developed as follows. In order to quantify the spatial extent of recycling processes, we introduce a characteristic length scale ℓ, henceforth referred to as the "recycling length." Physically, it marks the spatial range of recycling processes which effectively redistribute lipids across the membrane. Furthermore, $\ell \lesssim L_{cell}$, where L_{cell} denotes the linear dimension of a cell. At scales shorter than ℓ, the average composition is no longer conserved due to active lipid trafficking events, while the global composi-

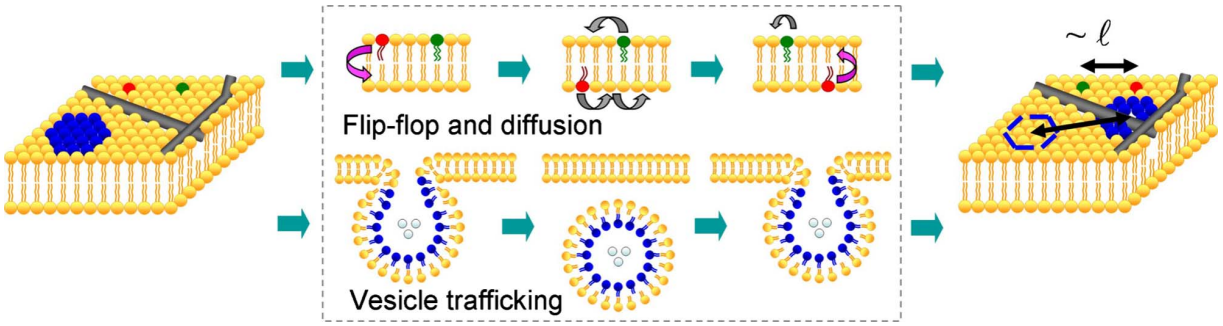

FIG. 1. (Color online) Schematic presentation of the nonequilibrium lipid transport processes considered here. Both protein-facilitated flip-flop events (upper pathway) and vesicle trafficking events between the plasma membrane and internal organelles (lower pathway) lead to an effective rearrangement of the lipid composition over a scale $\sim \ell$ in the exoplasmic leaflet. The gray tubes represent membrane compartmentalization.

tion is still conserved. Such processes can be incorporated to Eq. (7) via an additional noise term, which has the following properties: (1) in the vicinity of T_c, it reduces to temporal white noise, since any finite time correlations would appear almost instantaneous due to critical slowing down; (2) its spatial average is zero due to global mass conservation; (3) its spatial correlation length is given by ℓ; and (4) the redistribution of lipids occurs at a rate H. Thus, we propose the following (dimensionless) stochastic, nonlinear diffusion equation for the local composition within the exoplasmic leaflet in the presence of recycling,

$$\frac{\partial c(\mathbf{r},\tau)}{\partial \tau} = \nabla \cdot \{M \nabla [-\nabla^2 c - c + c^3 + g(\mathbf{r})]\} + \eta(\mathbf{r},\tau), \quad (8)$$

where η denotes a stochastic Gaussian noise with mean $\langle \eta \rangle = 0$ and correlator $\langle \eta(\mathbf{r}_1,\tau_1)\eta(\mathbf{r}_2,\tau_2)\rangle = -H^2/(2\pi)\nabla^2 K_0(|\mathbf{r}_1-\mathbf{r}_2|/\ell)\delta(\tau_1-\tau_2)$. $K_0(x)$ denotes a modified Bessel function of the second kind of the zeroth order. In Fourier representation, the noise correlator becomes $\langle \hat{\eta}(\mathbf{q},\tau_1)\hat{\eta}(\mathbf{q}',\tau_2)\rangle = \frac{H^2 q^2 \ell^2}{1+q^2\ell^2}(2\pi)^2\delta(\mathbf{q}+\mathbf{q}')\delta(\tau_1-\tau_2)$. By construction, the composition is nonconserved at spatial scales $\lesssim \ell$ and $\langle \hat{\eta}(\mathbf{q},\tau_1)\hat{\eta}(\mathbf{q}',\tau_2)\rangle \approx H^2(2\pi)^2\delta(\mathbf{q}+\mathbf{q}')\delta(\tau_1-\tau_2)$ for $q\ell \gg 1$, while the composition is conserved asymptotically with an effective "temperature" $T_{eff} = H^2\ell^2/(2k_B M)$ as dictated by the fluctuation-dissipation theorem (see, e.g., [74]).

In order to gain physical insight into some of the salient features of the recycling noise term, Fig. 2 displays noise realizations for $H=1$ and different ℓ values. The blue patches represent a local depletion of the raft component while the red ones represent a local increase. As expected, an increase in ℓ results in larger patches of the same color. Furthermore, as shown in Appendix A, the parameter H is related to the probability per unit time, p, that a given raft phase lipid is exchanged with a non-raft phase lipid (or vice versa) via $p = 3H^2 D(T_c - T)^2/(4A_{lipid}T_c^2)$. Here, A_{lipid} and D denote the area per lipid and diffusivity, respectively.

Finally, the additional term $g(\mathbf{r})$ in Eq. (8) describes a short-ranged interaction of lipids with the membrane proteins and the cytoskeleton, $g=0$ away from the protein or the cytoskeleton, while $g>0$ ($g<0$) denotes an attractive (repulsive) interaction for the raft phase in the vicinity of proteins or the cytoskeleton.

C. Analytical arguments

Before turning to numerical simulations, let us first paint a simple physical picture based on the general properties of Eq. (8). In terms of the recycling length ℓ, there are two limits amenable to simple analysis. First, consider the limit $\ell \to 0$ with $H\ell < (H\ell)_{crit}$. In this case, the coarsening dynamics takes over the stochastic fluctuations, leading to macroscopic phase separation. On the other hand, when $H\ell > (H\ell)_{crit}$, macroscopic phase separation is asymptotically negated as the renormalized temperature is above the critical temperature. As will be demonstrated below, in this noncoarsening regime both H and ℓ affect raft properties.

Next, consider the opposite limit $\ell \gg L$, where L denotes the linear dimension of the system. In this case, the noise correlator approximately takes the form $\langle \hat{\eta}(\mathbf{q},\tau_1)\hat{\eta}(\mathbf{q}',\tau_2)\rangle = H^2(2\pi)^2\delta(\mathbf{q}+\mathbf{q}')\delta(\tau_1-\tau_2)(1-\delta_{\mathbf{q},0})$, independent of the value of ℓ. Here the term $(1-\delta_{\mathbf{q},0})$ ensures that the composition is globally conserved. If this constraint is relaxed, the average global composition undergoes large fluctuations. This can be seen by considering the time evolution of the average global composition, which is only affected by the noise term, as the deterministic part of the equation conserves mass. Indeed, by taking the Fourier transform on both sides of Eq. (8), in the limit, $\mathbf{q} \to \mathbf{0}$, we have $\partial \hat{c}(\mathbf{q},\tau)/\partial\tau = \hat{\eta}(\mathbf{q},\tau)$. The Fourier transform of the first term on the right

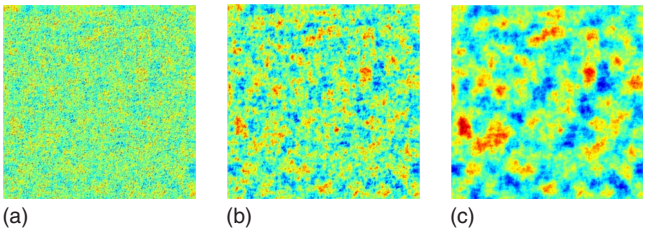

FIG. 2. (Color online) Instantaneous recycling noise term realizations with different recycling lengths: (a) $\ell = 0.01$, (b) $\ell = 2$, and (c) $\ell = 128$. The red, light grey in print (blue, dark grey in print) patches represent a local depletion (increase) of the raft component. The data has been locally averaged over a circular area of radius $r=10$ to highlight the differences in the large scale behavior between the three examples. Note that an increase in ℓ results in larger patches of the same color.

hand side of Eq. (8) vanishes since it is $\sim O(q^2) \to 0$ as $\mathbf{q} \to 0$. We then calculate

$$\langle |\hat{c}(\mathbf{q})|^2 \rangle = \langle \int_0^\tau \int_0^\tau \hat{\eta}(\mathbf{q},\tau_1)\hat{\eta}(\mathbf{q},\tau_2) d\tau_1 d\tau_2 \rangle = \int_0^\tau \int_0^\tau \langle \hat{\eta}(\mathbf{q},\tau_1)\hat{\eta}(\mathbf{q},\tau_2)\rangle d\tau_1 d\tau_2 = H^2\tau,$$

implying that the average global composition exhibits random walk in time. In particular, $\lim_{\tau\to\infty}\langle |\hat{c}(\mathbf{q})|^2\rangle \to \infty$ as $\mathbf{q} \to 0$. This implies the presence of long-ranged (algebraic) correlations and self-similar spatial structures [78]; it also leads to a broad domain size distribution. Thus, a sufficiently rapid recycling rate (large H) and/or long-ranged (large ℓ) lipid exchange processes are required to counteract the coarsening dynamics.

We now describe the physical picture that emerges from the above analysis. At fixed ℓ, there are two possibilities. First, when $(H\ell) < (H\ell)_{crit}$, the coarsening dynamics is dominant, and the system equilibrates by continuous coarsening of the raft domains. In this regime, fluctuations due to recycling simply renormalize the surface tension [75]. We call this "the coarsening regime," and argue that it accounts for the experimental observations of macroscale phase separation in synthetic membranes [30,31]. On the other hand, in the regime $(H\ell) > (H\ell)_{crit}$, the recycling processes dominate over the coarsening dynamics. In this case, we expect any domain with linear dimension $L \gg \ell$ to fragment since the effective temperature restricts the system above the miscibility gap. Physically, this implies that phase separation at scales $\gg \ell$ is suppressed. For spatial scales below ℓ, however, we expect a broad size distribution of domains to form due to the effective nonconserved nature of the recycling noise term. The domains coarsen and fragment in a highly dynamic fashion due to the competition between the line tension (which promotes coarsening) and the lipid trafficking events (which promotes fragmentation). Hence, we call it "the noncoarsening regime." As will be shown in the next Section, this physical picture is supported by the full numerical simulations of the model.

III. SIMULATION RESULTS

Before turning to the description of the results from numerical simulations, we first present the numerical scheme employed in the simulations. The numerical scheme is then applied to elucidate raft formation in the presence of recycling, membrane compartmentalization, and membrane proteins.

A. Numerical scheme

Finite differencing was adopted for both spatial and temporal derivatives in the discrete version of Eq. (8),

$$c_{i,j}(\tau+\Delta\tau) = c_{i,j}(\tau) + \Delta\tau\{\nabla\cdot[M\nabla\mu(c)]\}_{i,j} + \eta_{i,j}(\tau), \quad (9)$$

where

$$(\nabla\cdot[M\nabla\mu(c)])_{i,j} = \left[\frac{M_{i+1,j}+M_{i,j}}{2}\frac{\mu_{i+1,j}-\mu_{i,j}}{\Delta x^2} - \frac{M_{i,j}+M_{i-1,j}}{2}\frac{\mu_{i,j}-\mu_{i-1,j}}{\Delta x^2} + \frac{M_{i,j+1}+M_{i,j}}{2}\frac{\mu_{i,j+1}-\mu_{i,j}}{\Delta y^2} - \frac{M_{i,j}+M_{i,j-1}}{2}\frac{\mu_{i,j}-\mu_{i,j-1}}{\Delta y^2}\right], \quad (10)$$

and

$$\mu_{i,j} = -\frac{c_{i+1,j}+c_{i-1,j}-2c_{i,j}}{\Delta x^2} - \frac{c_{i,j+1}+c_{i,j-1}-2c_{i,j}}{\Delta y^2} - c_{i,j} + c_{i,j}^3 + g_{i,j}. \quad (11)$$

The computational domain is $L\times L$ with periodic boundary conditions with $L=256$ unless otherwise stated; the results discussed in this paper did not display any detectable finite-size effects. The initial composition was chosen to be homogeneous with small random fluctuations drawn from a Gaussian distribution. Finally, the discretized noise term $\eta_{i,j}(\tau)$ is obtained by the inverse discrete Fourier transform of $(H\sqrt{\Delta\tau}/\Delta x)\ell|\mathbf{q}|/\sqrt{1+\mathbf{q}^2\ell^2}\times\hat{\zeta}(\mathbf{q},\tau)$, where $\hat{\zeta}(\mathbf{q},\tau)$ is the Fourier transform of a discrete Gaussian random field with mean $\langle\zeta_{i,j}(\tau)\rangle=0$ and variance $\langle\zeta_{i,j}(m\Delta\tau)\zeta_{i',j'}(n\Delta\tau)\rangle = \delta_{i,i'}\delta_{j,j'}\delta_{m,n}$.

In this work, dimensionless time step $\Delta\tau=0.005$ and grid spacing $\Delta x=\Delta y=1$ were employed. We verified that the simulation results have converged with respect to both of these choices, both qualitatively and quantitatively. To this end, Fig. 3 displays two representative snapshots with $H=1.41$, $\ell=\infty$ and $\phi=0$, and $(\Delta x,\Delta\tau,L)=(0.5,0.0013,512)$ for (a) and (1,0.005,256) for (b), respectively. As can be seen, the steady-state morphologies appear very similar. More quantitatively, we also computed the mean domain size from

$$R(\tau) \equiv 2\phi L^2/L_B(\tau), \quad (12)$$

where $L_B(\tau)$ denotes the total domain interface length at time τ and $\phi=(1-\bar{c})/2$ is the nominal raft area fraction; here, $\bar{c}$ denotes the spatially averaged concentration, which is conserved by the dynamics in Eq. (8). We note that the true raft area fraction may vary due to stochastic fluctuations in the composition field or due to local accumulation of the raft phase in the presence of raft-attracting membrane proteins. The data, shown in Fig. 3(c), clearly demonstrates that the steady-state domain size $\lim_{\tau\to\infty} R(\tau)\equiv\bar{R}$ has converged within the error bars for three different choices for the grid spacing Δx and time step $\Delta\tau$. Finally, we note that a comprehensive discussion of the effects of time step and grid spacing on the numerical solution of Eq. (8) in the limit $\ell\to 0$ at constant mobility and in the absence of the term $g(\mathbf{r})$ can be found in [77].

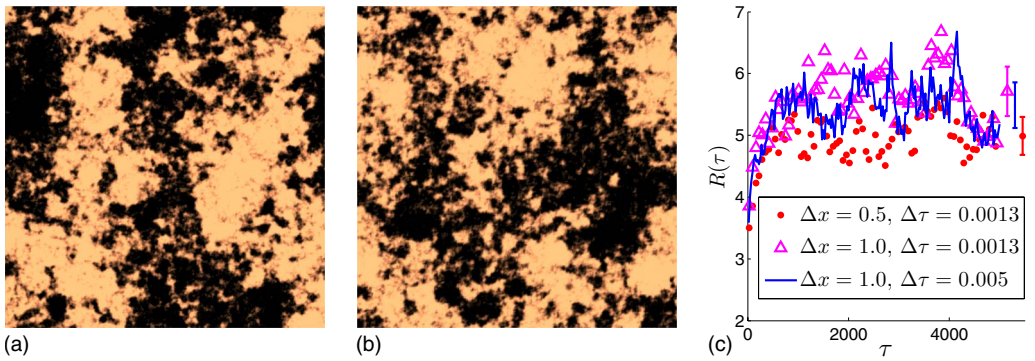

FIG. 3. (Color online) Snapshots of domain configurations with different Δx and $\Delta\tau$ in steady state. Raft and nonraft phases are shown in black and copper, respectively. (a) $\Delta x=0.5$, $\Delta t=0.0013$ and (b) $\Delta x=1.0$, $\Delta t=0.005$. The other parameters were set to $H=1.41$, $\ell=\infty$, and $\phi=0$ for both simulations. (c) The asymptotic domain size converges for different choices of the grid spacing Δx and time step $\Delta\tau$ within error bars, which are shown for the three data points corresponding to the end of the simulations.

B. Coarsening vs noncoarsening regimes

To verify the analytical arguments regarding the presence of $(H\ell)_{crit}$ delineating the coarsening regime from the noncoarsening one, Eq. (9) was iterated for H ranging from 0.14 to 1.41, and ℓ ranging from 2 to 1280. To showcase the results, we discuss two specific choices of parameters, (1) $H=0.71$ and $\ell=1$, and (2) $H=0.71$ and $\ell=64$, see Fig. 4. The former choice of parameters leads to domain coarsening while the latter leads to the noncoarsening, steady-state regime, see Fig. 5.

In the coarsening $[H\ell<(H\ell)_{crit}]$ regime, the domains keep growing with time consistent with the expected $R \sim \tau^{1/3}$ scaling. In the noncoarsening regime, on the other hand, the domain size approaches a constant value, $\bar{R}(\ell,H,\phi)$. The results are in agreement with the critical $H\ell$ argument: below $(H\ell)_{crit}$, the domains keep growing, while above $(H\ell)_{crit}$ the average domain size saturates to a value independent of the system size. As a result, small raft domains exist only when the recycling processes are strong enough to counteract the coarsening process. With regard to the value of $(H\ell)_{crit}$, our simulation results imply $(H\ell)_{crit}=2.1\pm0.4$. In the remainder of the paper, we will focus on the noncoarsening regime relevant for raft formation and regulation.

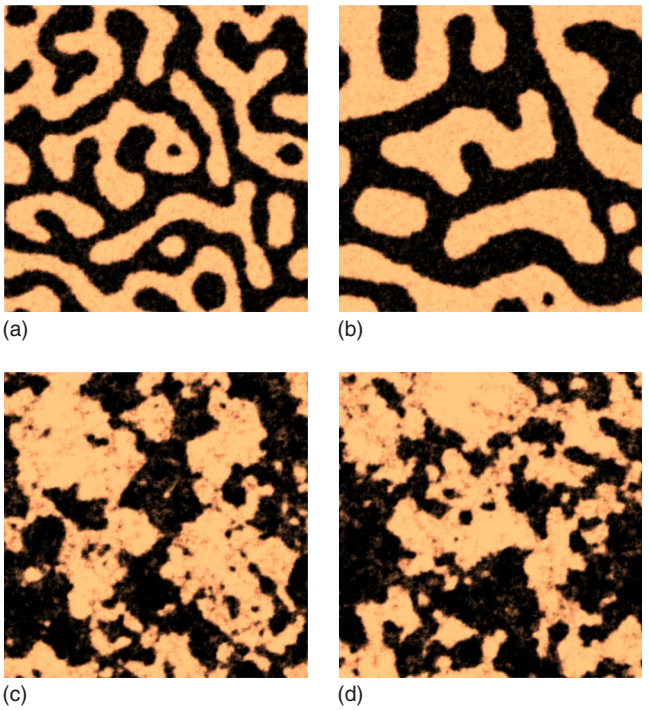

FIG. 4. (Color online) Snapshots of domain configurations with different recycling lengths with $\ell=1$ (a) and (b) and $\ell=64$ (c) and (d). Raft (nonraft) phase is shown in black (copper). The snapshot times are $\tau=2000$ (a) and (c) and $\tau=7500$ (b) and (D=d). For both systems, $\phi=0.5$ and $H=0.71$.

C. Nonequilibrium membranes: recycling, membrane compartmentalization, and membrane proteins

Let us next turn to a discussion of the roles of recycling, membrane compartmentalization, and immobile raft-attracting/repelling proteins on the global and local raft domain regulation.

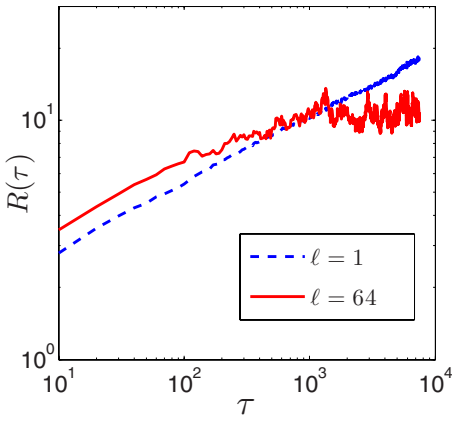

FIG. 5. (Color online) The time evolution of the mean domain size corresponding to Fig. 4. Continuous domain coarsening is observed for $\ell=1$ with $R\sim t^{0.29\pm0.02}$, while for $\ell=64$ domain coarsening is suppressed and the system enters a steady-state due to sufficiently strong recycling processes.

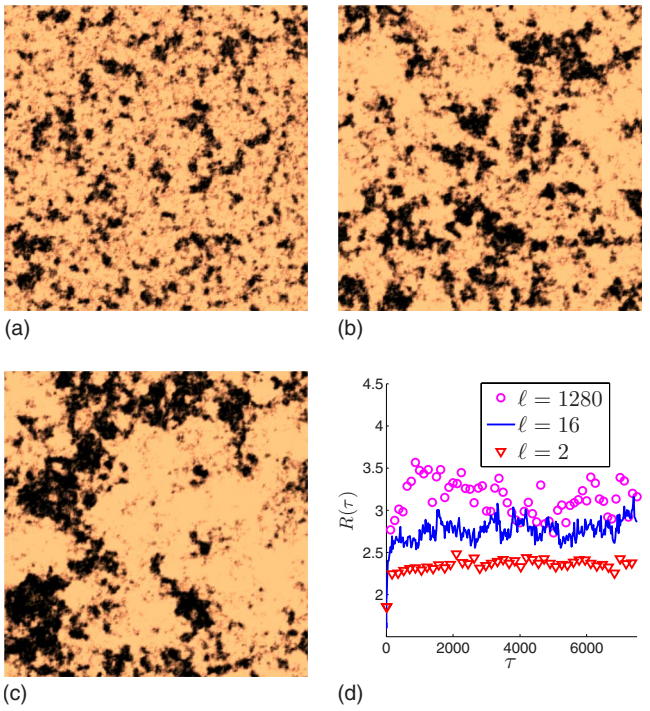

FIG. 6. (Color online) Snapshots of domain structures in steady state with recycling lengths (a) $\ell=2$, (b) $\ell=16$, and (c) $\ell=1280$. For all cases, $\phi=0.25$ and $H=1.41$. Again, the raft (nonraft) phase is shown in black (copper). (d) The average domain size in steady state increases as ℓ increases.

1. Global raft domain regulation

In this part we will quantify the dependence of the mean domain size $\bar{R}$ on the recycling length ℓ, rate H, and raft area fraction ϕ. First, the dependence of $\bar{R}$ on ℓ is examined. Figure 6 displays typical domain structures in the steady state with different recycling lengths. The snapshots reveal two important characteristic features of the model. First, the raft domains have irregular shapes. Second, systems with larger ℓ sustain larger raft domains in the steady-state regime. Furthermore, careful observations of time-dependent domain morphologies reveal that small raft domains have short lifetimes while larger domains persist much longer.

To quantify the dependence of $\bar{R}$ on ℓ, the steady-state raft domain area distribution $P(A)=N_A/N_{total}$, in which N_A is the number of raft domains of size A and N_{total} the total number of raft domains, has been determined. A raft domain is defined as a continuous region in which $c<0$, and the minimum size for a raft is a single point ($A=1=\Delta x^2$). The data for $P(A)$ versus A are displayed in Fig. 7 (a) on a logarithmic scale. Figure 7(b), on the other hand, shows that ℓ essentially provides a large scale cutoff for $P(A)$; that is, the formation of domains larger than $\sim\ell$ in linear dimension is strongly suppressed. Note also that $P(A)\sim A^{-\alpha}$ for $1<A\ll\ell^2$, where $\alpha\approx 1.6\pm 0.1$. We have verified that α is independent of H and ϕ when coarsening is suppressed. Thus, the scaling of the average domain area in terms of ℓ is given by $\langle A\rangle \sim \ell^{2(2-\alpha)}$, which implies that $\bar{R}\sim\ell^{2-\alpha}=\ell^{0.4}$. In other words, $\bar{R}$ is only weakly dependent on ℓ. Finally, the distribution

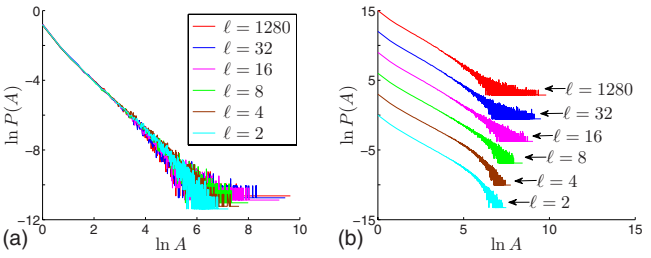

FIG. 7. (Color online) The behavior of domain size distribution for lipid raft area fraction $\phi=0.25$ and $H=1.41$ for several values of the recycling length ℓ on a logarithmic scale. The data in (b) have been shifted vertically to highlight the observations that (1) the different curves have the same slope, as can be seen in (a), and (2) the main effect of increasing the recycling length ℓ is to allow for the formation of larger domains, highlighted in (b).

$P(A)\sim A^{-\alpha}$ is broad in the sense that extrapolating to $\ell\to\infty$ and $L\to\infty$ leads to $\bar{R}\to\infty$ when $\alpha<2$; that is, the mean over the distribution diverges.

In Fig. 8, sample domain configurations and the corresponding mean domain sizes are displayed for a fixed raft area fraction or recycling rate. The data shows that increasing the recycling rate leads to a smaller mean domain size $\bar{R}$ at constant raft area fraction ϕ. In a similar manner, for a fixed recycling rate, increasing the raft area fraction leads to a larger mean domain size $\bar{R}$. To quantify these conclusions,

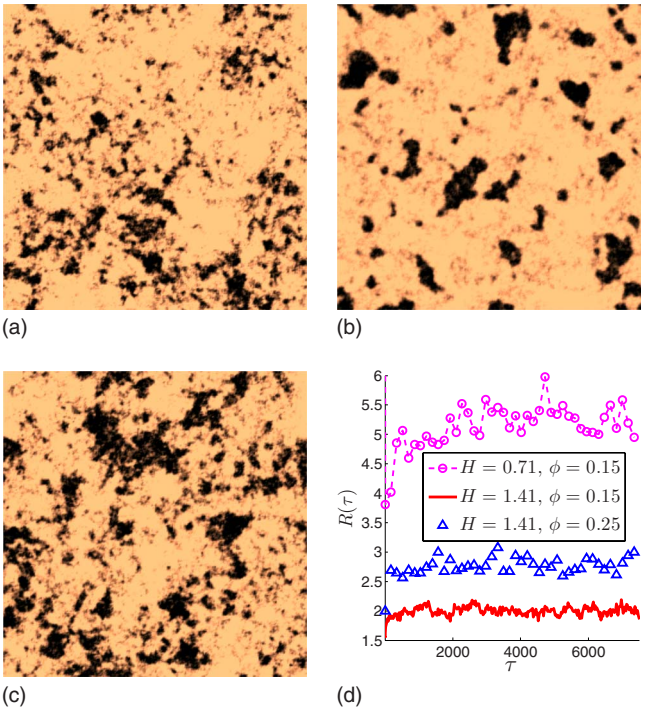

FIG. 8. (Color online) Snapshots of domain structures in steady state. The recycling rate $H=1.41$ (a) and (c) and $H=0.71$ (b). The nominal lipid raft area fraction was set to $\phi=0.15$ (a) and (b) or 0.25 (c), with the recycling length $\ell=16$. Again, the raft (non raft) phase is shown in black (copper). The average domain size plotted in (d) shows that the average domain size decreases as the recycling rate increases and/or area fraction decreases.

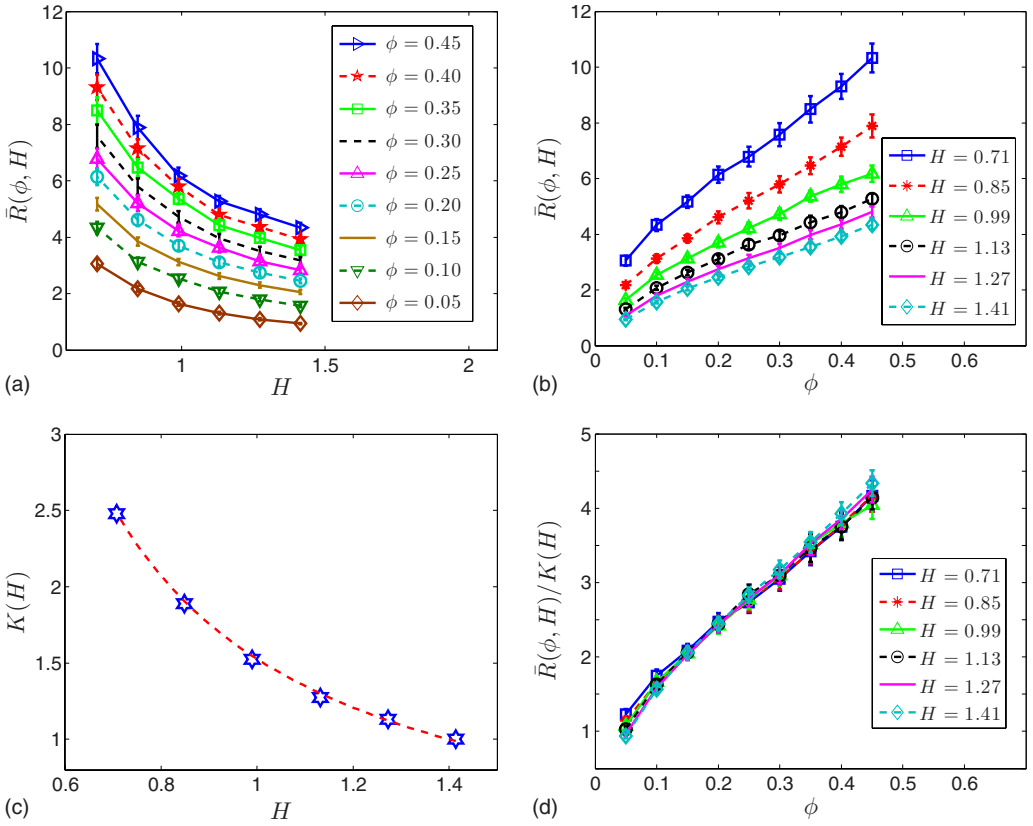

FIG. 9. (Color online) Steady state domain size $\bar{R}$ as a function of H, ϕ, and the scaling of the data. (a) $\bar{R}$ vs H for a fixed ϕ; (b) $\bar{R}$ vs ϕ for a fixed H; (c) $K(H)$ vs H. The red line is a fitting function for $K(H)$; (d) $\bar{R}(\phi,H)/K(H)$ vs ϕ. Recycling length $\ell=20$ for all simulations.

the mean domain size $\bar{R}(\phi,H)$ for several H and ϕ values are plotted in Figs. 9(a) and 9(b). The shapes of the curves suggests that $\bar{R}(\phi,H)$ has a decoupled dependence on H and ϕ. We thus propose that, in the limit $H\ell \gg (H\ell)_{crit}$, the mean domain size has the simple scaling form $\bar{R}(H,\phi) = K(H)Y(\phi)$, where K and Y are functions of H and the lipid raft area fraction ϕ, respectively. Examination of the numerical data presented in Figs. 9(c) and 9(d) reveals that the scaling ansatz is obeyed over the entire parameter range we have explored. Although, we have been unable to derive the functional forms for the scaling functions K and Y, we have found empirically that they are well approximated by $K(H) \sim 1/(H-\text{Const.})$ and $Y(\phi) \sim \sqrt{\phi/(1-\phi)}$.

Figure 10 visualizes further the implications of the ℓ and H dependency of $\bar{R}$ discussed above. In Fig. 10, it can be seen that $\bar{R}$ increases monotonically when H decreases. On the other hand, for a fixed H and varying ℓ, $\bar{R}$ has a weakly nonmonotonic behavior, with a rapid initial decrease followed by a rather slow increase as ℓ increases. Theoretically, we would expect $\bar{R} \sim \ell^{0.4}$ in this regime, as discussed above. When $\ell > \ell^*$, the system approaches a steady state. Upon increasing ℓ, $\bar{R}$ first decreases since the coarsening is suppressed, and then increases as larger and larger domains form in the system. When $\ell < \ell^*$, the system is in the coarsening regime. Thereby no data points are plotted for this region in Fig. 10. Of course, this implies that upon approaching the critical $H\ell$, the assumed scaling form for $\bar{R}$ no longer holds.

The values presented in Figs. 3, 5–12, and 14 are in dimensionless units. In order to obtain practical insight to the significance of the results, we next carry out a conversion back to physical units. Using lipid diffusion constant value $D=10^{-13}$ m^2/s [79], $T_c=310$ K, $T_c-T=1$ K, $A_{lipid}=10^{-18}$ m^2 [80], and $p=0.8$/s, while ℓ varies from $\ell=100$ nm to $\ell=200$ nm, for example, the green dashed line in Fig. 10 at the right top corner corresponds to an average domain size of 40 nm, which is well within the experimental domain size results region of 20 nm–200 nm in plasma membrane [20–25]. In short, the explorations of $\bar{R}$ suggest that the

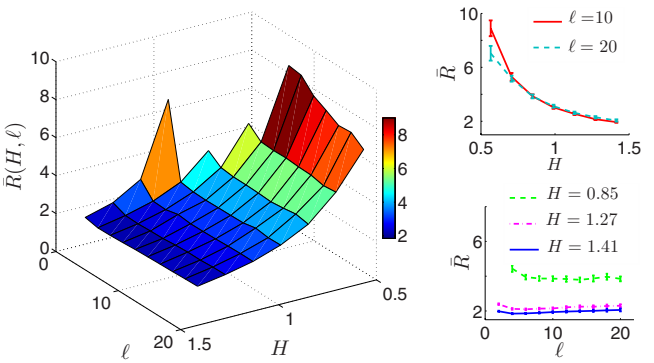

FIG. 10. (Color online) Steady-state average linear domain size as a function of the recycling rate H and length ℓ for a fixed nominal lipid raft area fraction $\phi=0.15$. Note that H increases from right to left in the plot. The two frames on the right display slices through the data at fixed H and ℓ, respectively.

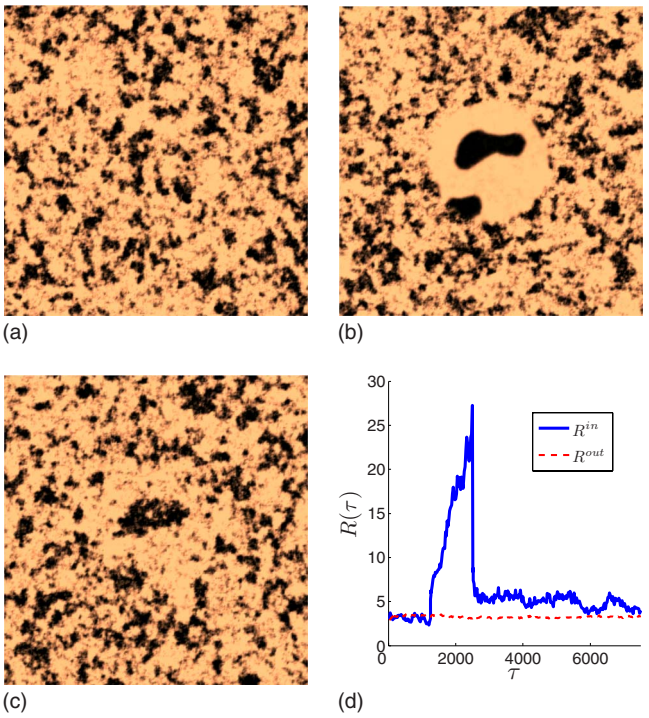

FIG. 11. (Color online) Effect of spatiotemporally varying H on local raft domain properties. At the center of the system inside a disk of radius $r=50$, $H^{in}=0.25$ for $1250 \leq \tau \leq 2500$, while $H^{in}=1.41$ at all other times; outside the disk, $H^{out}=1.414$ always. The lipid raft area fraction $\phi=0.3$ and the recycling length $\ell=4$ everywhere. The plot in (d) shows the time development of $R(\tau)$ inside and outside the disk region [$R^{in}(\tau)$ and $R^{out}(\tau)$, respectively]. The snapshots were taken at (a) $\tau=1000$, (b) $\tau=2400$, and (c) $\tau=2525$, respectively. Note that $R^{in}(\tau)$ rapidly increases in the time window when H^{in} is reduced, and rapidly decreases toward the steady-state value when H^{in} is reset to its original value.

mean domain size could be regulated by varying the recycling rate, the length or the rafts area coverage. Furthermore the domain size distribution is always broad. Finally, the lifetime of raft domains has a broad distribution as well, and will be addressed in a separate publication [81].

2. Local raft domain regulation

The results discussed above suggest that cells may regulate the *global* raft domain properties by altering the global recycling rate, length, or raft area fraction, or combinations thereof. In light of experimental evidence for spatial localization of raft domains [82–84], it is thus interesting to explore the possibility that the cell may be able to regulate *local* raft domains by spatially varying H, ℓ, or ϕ. To this end, we have run simulations with a spatially and temporally varying H in a simplified geometry. More specifically, initially we set $H=1.41$ everywhere. At $\tau=1250$, H is reduced to a much smaller value ($H=0.25$) inside a circular region of radius $r=50$, while the recycling rate remains unchanged everywhere else. At $\tau=2500$, the recycling rate is set back to $H=1.41$ inside the disk. Snapshots from the simulation are shown in Fig. 11 together with the time dependent raft domain size inside and outside the disk, respectively.

It can be seen in Fig. 11 that between $\tau=0$ and $\tau=1250$, the local raft domain size within the disk is indistinguishable from that outside the disk. Between $\tau=1250$ and $\boldsymbol{\tau}=2500$, however, the situation is dramatically different: a local decrease in the recycling rate promotes domain coarsening, and transient large raft clusters appear within the disk. Upon increasing the recycling rate within the disk back to its original value leads to rapid fragmentation of the large clusters and the domain size properties quickly approach those outside the disk.

Interestingly, if the low-recycling rate is maintained for a much longer time, it is found that raft domains vacate the disk altogether. This can be explained by the following simple argument. Since the effective temperature is lower within the disk than outside the disk, the line tension between the raft and nonraft domains is higher within the disk than outside. Therefore, from thermodynamic considerations, it would be much more preferable to localize the compositional domains in the high temperature regions—i.e., outside the disk. This suggests that temporary changes in the local recycling rate can be employed to regulate local raft domain structure in a transient manner, while permanent changes may lead to large variations in the local raft area fraction.

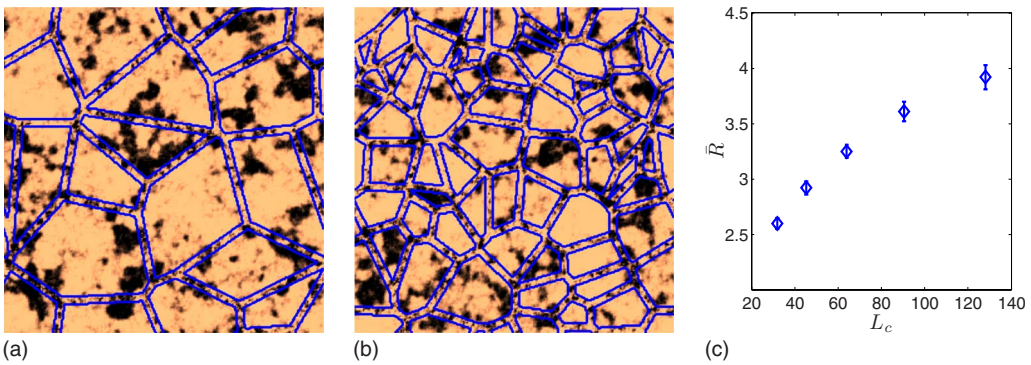

FIG. 12. (Color online) Snapshots of domain structures and the mean domain size evolution in the presence of compartments of characteristic linear dimension (a) $L_c=64$ and (b) $L_c=32$ with compartment boundaries described by a reduced mobility. In the simulations $\phi=0.25$, $H=0.85$, and $\ell=10$. The mobility M reduces from a value of $M=1$ inside the compartments to $M=0.1$ at the compartment boundaries, whose thickness was set to 6 grid spacings. As can be seen from (c), the domain size decreases as L_c decreases, corresponding to an increase in the total compartment boundary length.

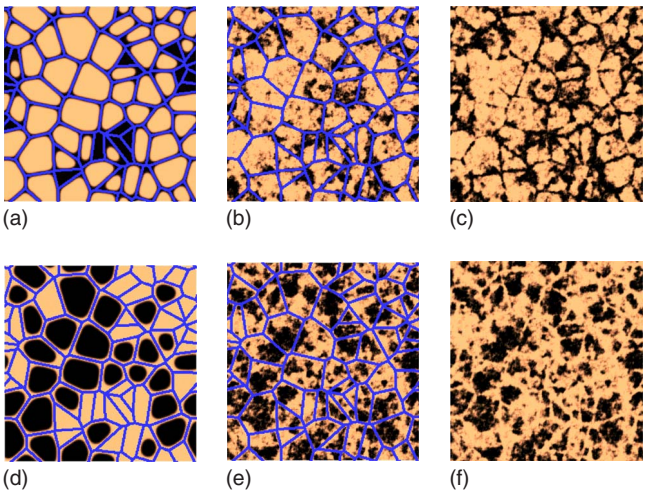

FIG. 13. (Color online) Snapshots of domain configurations in the presence of compartment boundaries (not drawn to scale), represented by a nonzero value of $g(r)$, which either attract [(a) ~ (c)] or repel [(d) ~ (f)] the raft phase. $g(r)=0.8$ for [(a) ~ (c)] and $g(r)=-0.8$ for [(d) ~ (f)]. Except for the boundaries represented by the blue mesh, $g(r)=0$ elsewhere. No recycling is present in (a) and (d), while $H=1.13$ and $\ell=10$ in (b), (c), (e), and (f); furthermore, to assist in viewing, (c) and (f) display only the local composition from snapshots (b) and (e), respectively, with compartment boundaries excluded. Compartment boundary thickness is 3, and the nominal raft area fraction $\phi=0.4$. Note that the boundary-lipid interaction has shifted the equilibrium compositions of the raft and nonraft phases, and thus, the effective raft area fraction varies between frames.

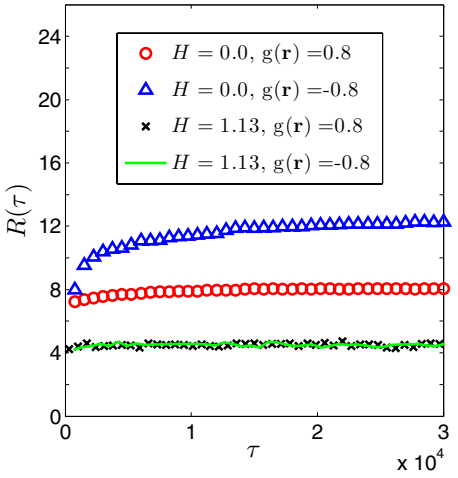

FIG. 14. (Color online) Average domain size in the presence of compartments with attractive or repulsive raft-boundary interactions.

3. Compartmentalization

Next, we turn to the possible role of membrane compartmentalization on raft formation. Indeed, in single particle tracking experiments, lipid molecules have been found to undergo "hop" or "confined" diffusion [25,85]. It is suspected that hop diffusion is caused by confinement of the lipid molecules into compartments either by a mesh formed by the actin-based membrane cytoskeleton or the membrane cytoskeleton-anchored proteins [86]. To study the effect of this compartmentalization on domain formation, we focus on two scenarios for the role of the compartments: (1) they may act as diffusion barriers by having a lower effective lipid diffusivity, or (2) they may energetically either attract or repel the raft phase. In both cases, the cell membrane is assumed to be compartmentalized by a network generated using a Random Poisson process Voronoi scheme [87], as illustrated in Figs. 12 and 13.

We start with the first scenario involving diffusion barriers. In this case, the mobility field is modulated via a step function such that it reduces from $M=1$ inside the compartments to $M=0.1$ within the compartment boundaries with no dependency on c. Figure 12 shows the results related to two sample network configurations containing compartments of characteristic linear dimension $L_c=64$ and $L_c=32$ with a boundary thickness of 6 in units of the grid spacing, respectively. As expected, reduced mobility within the compartment boundaries reduces the mean raft size. Physically, this results from the fact that the lower mobility within the boundaries leads to more sluggish local domain growth. Therefore, the domains crossing the boundaries are smaller than those residing with the compartments. As a result, the overall average domain size decreases as the total compartment boundary length increases, shown in Fig. 12(c). Effectively, the compartment boundaries act as "scissors" that cut the raft domains into smaller pieces, and a larger compartment boundary area fraction leads to more effective fragmentation of the raft domains and thus smaller mean raft domain size.

In the second scenario, the mobility remains unchanged, but we turn on the interaction between lipids and the compartment boundaries. Specifically, $g(\mathbf{r})$ in Eq. (8) is nonzero at the compartment boundaries such that $g(\mathbf{r})>0(<0)$ represents an attraction (repulsion) between the mesh and the raft domains. Representative snapshots are shown in Fig. 13 for $g=0.8$ and $g=-0.8$ within the compartment boundaries and at different recycling rates and lengths. Interestingly, in the absence of recycling, a strong enough boundary-lipid interaction will localize either the raft or the nonraft phase, depending on the sign of the interaction; estimates for the critical interaction strengths are derived in Appendix B. That is, the raft-compartment boundary interaction may stabilize finite-sized raft domains in thermodynamic equilibrium [see Figs. 13(a) and 13(d)]. When $g(\mathbf{r})$ is weaker than the critical value, however, the interaction is not sufficient to constrain the spatial distribution of the raft domains in equilibrium.

In the presence of recycling processes, the raft domains are less constrained by the boundaries, as can be seen in Figs. 13(b) and 13(e). As expected, increasing the recycling rate tends to wash out the localization effect of the compartment boundaries. Interestingly, the data for mean domain sizes, computed from Eq. (12) and shown in Fig. 14, indicates that although raft domain morphologies are strongly dependent on whether the boundaries are attractive or repulsive, their characteristic size does have only a rather weak dependence on the nature of the raft-boundary interaction even in the absence of recycling. Also, when the raft do-

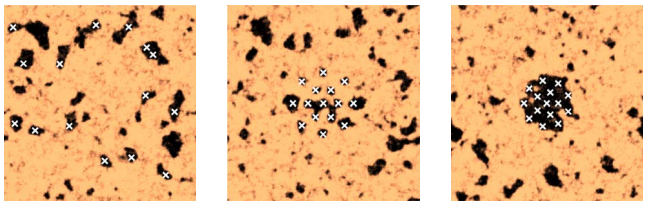

FIG. 15. (Color online) Spatial localization and aggregation of lipid rafts due to membrane proteins. Here, white crosses indicate the locations of immobile membrane proteins. (a) Raft distribution in the presence of 15 randomly distributed proteins. Notice how each protein is surrounded by a raft domain. (b) Raft distribution in the presence 15 weakly clustered proteins. (c) Raft distribution in the presence of 15 strongly clustered proteins. Note the appearance of an extended raft centered around the protein aggregate in the right panel.

mains are strongly repelled by the boundaries, a decrease in the compartment size will lead to a decrease in the mean domain size as the compartment size sets the maximum domain size.

In all, these results suggest that a strong raft-boundary interaction may control (or at least influence) both the spatial distribution of rafts and their mean size. However, if recycling processes are present, the size controlling effects due to the mesh interaction may be reduced, and a large enough recycling rate would completely overwhelm the boundary interaction. These observations indeed support the notion that the raft size and spatial distribution are dependent on the cytoskeleton as suggested in [25]. It is also interesting to note that while such boundary-lipid interactions might indeed stabilize rafts in thermal equilibrium, the raft domains would not be very dynamic entities, and thus would be difficult to rationalize in light of experiments displaying transient confinement [25,85].

4. Immobile raft-attracting membrane proteins

Finally, we turn to a discussion of the role of immobile raft-attracting membrane proteins on raft formation. In particular, here we assign a favorable interaction between the proteins and the raft phase; such an interaction would thus tend to spatially localize the raft domains. Indeed, this is what we find. We start by placing 15 immobile proteins along the membrane with a varying degree of clustering such that $g=0.5$ within a small disk of radius 5 around the proteins and $g=0$ elsewhere; the other parameters were set to $\phi=0.15$, $H=0.71$, and $\ell=8$. Representative snapshots are presented in Fig. 15. In the absence of protein clustering, each protein is surrounded by a stable raft domain. Although the mean raft domain size is not affected by the proteins, the presence of proteins still leads to spatially localized rafts, as shown in Figs. 15(a) and 15(b). Upon increasing the clustering of proteins, an extended raft aggregate emerges [Fig. 15(c)]. These observations imply that the clustering of proteins may indeed contribute to the aggregation of rafts, as discussed in [8,19,88]. Such clusters of proteins in cholesterol-rich domains have also been observed within the cytoplasmic leaflet of the plasma membrane in recent experiments [29].

IV. DISCUSSION AND CONCLUSIONS

In this paper, we have argued that rapid lipid recycling coupled to a tendency to phase separate provides a robust mechanism for establishing a steady state, in which the compositional rafts domains attain a finite size in the exoplasmic leaflet of the plasma membrane. To this end, we constructed a continuum phase field model by incorporating the nonequilibrium stochastic lipid recycling processes to a standard phase separation model. The two important parameters in our model arising from the lipid recycling processes are the recycling rate H and length ℓ. At large length scales $\gg\ell$, the recycling processes simply appear as an effective temperature, and if this temperature is high enough, macroscopic phase separation is suppressed and the system is *globally miscible* due to the competition between the thermodynamic driving force (promoting phase separation) and lipid recycling (resisting phase separation). However, at length scales $\ll\ell$, the system is *locally immiscible* and undergoes *local* phase separation, resulting in fluctuating finite-sized raft domains. On the other hand, if the recycling rate or length is reduced sufficiently, the system eventually becomes *globally immiscible* and macroscopic phase separation ensues.

While similar ideas based on lipid recycling have been proposed in the past by others [47,50,53,54], the model presented here is the first that incorporates both the spatial distribution of the raft domains and their morphologies, as well as their interaction with membrane compartments and membrane proteins. It is noteworthy that the raft domain size distribution is broad (ranging from tens to hundreds of nanometers) in both our approach and in that of [50], consistent with experimental observations [20,22,23]. Furthermore, the rafts in our model are highly dynamic entities with varying life times with larger rafts persisting longer than smaller rafts, again consistent with experimental results [20,23,24].

We also explored the domain size dependence on the recycling rate, recycling length, and raft area fraction. In our approach, the recycling rate and length are two important parameters which incorporate lipid recycling processes, such as flip-flop, translocation, or vesicle trafficking [89–93]. Although a detailed relation between the recycling rate H and the kinetics of the above processes is too complex to derive, intuitively a smaller H corresponds to slower processes. Our simulation results show that a decrease in the recycling rate leads to larger raft domains, in agreement with Refs [50,53,54]. This suggests that in experiments, slowing down such recycling processes might induce larger rafts. Interestingly, a similar result regarding membrane proteins has been reported in [94], in which the inhibition of endocytosis and vesicle trafficking induced larger class I HLA protein clusters. Furthermore, we found that the average raft domain size decreases as the raft area fraction decreases. In experiments, indirect support of the conclusion is available: in [19–21,25,26,28] the depletion of cholesterol or sphingolipids caused a decrease in the confinement zone size which potentially corresponds to rafts enriched in these molecules

[6,7]. Finally, we proposed that cells could regulate the *local* raft size by varying the recycling processes spatially and temporally in polarized cells, in which lipids and proteins are sorted and transported to different parts of the membrane to maintain membrane polarity [82–84].

In addition, we investigated the role of membrane compartmentalization on raft size distribution and dynamics. We focused on two plausible scenarios, one in which the compartment boundaries act as diffusion barriers and another in which the boundaries attract or repel the raft domains; experimental evidence for the former scenario exists [95–99], while the latter one is speculative at this point. In both scenarios, the local recycling processes were assumed to remained unchanged. In the former case, smaller raft domains appeared at the compartment boundaries, since the coarsening process locally slows down. Thus, diffusion barriers tend to fragment large raft aggregates. In the second scenario, we observed that the lipid-boundary interaction greatly affects the spatial distribution of rafts, while the effects on the mean raft size depends on the interaction strength only very weakly. We conclude that the cytoskeleton related compartmentalization could regulate the size and spatial distribution of rafts, which is consistent with the experiments in [100], where it was found that raft domains do not form if the actin cytoskeleton is disassembled. Meanwhile, in [25] it was shown that both rafts and the cytoskeleton influence confined diffusion. Together with our results, these observations indicate that the raft distribution could be regulated by the cytoskeleton and that the cytoskeleton could directly or indirectly confine particle diffusion.

Finally, we probed the effects of immobile membrane proteins on raft formation, spatial localization, and dynamics. It is well known that some membrane proteins have an affinity to the l_o raft phase [7,101–103] and, therefore, rafts may play a role in signal transduction [7–10]. However, it is unclear whether the raft phase recruits proteins or whether the proteins cause the rafts to form by recruiting lipids. The former scenario has been proposed in [9,10,104–106], in which rafts have been proposed to recruit or prevent the aggregation of signaling proteins, which could then facilitate or inhibit signal transduction. On the other hand, [28,88,107–109], propose that the aggregation of proteins may cause further aggregation and stabilization of transient rafts. In both cases, a protein-raft interaction is involved. We incorporated this interaction to our model, and the simulation results show that isolated protein may localize raft domains while a protein cluster may facilitate the formation of spatially extended rafts. These observations are consistent with both the views of a raft recruiting proteins and the views of a protein cluster stabilizing the raft phase. Indeed, if the proteins attract the raft phase, the reverse must also be true. Thus, we conclude that an affinity between proteins and the raft domains is a requirement for both scenarios, but that further work is required to conclusively determine, which scenario is the prevalent one.

In summary, in this paper we have studied the roles of lipid trafficking, compartmentalization, and protein-lipid interactions on lipid raft formation process in the plasma membrane. First, we argued that nonequilibrium processes, such as lipid trafficking and recycling, provide a robust mechanism for establishing a finite size distribution of compositional raft domains in an immiscible lipid system, and presented a physically based model to explain raft domain formation in the plasma membrane. Numerical simulations of the model and simple analytical arguments were employed to demonstrate the presence of non equilibrium steady states, in which the raft domains attain a finite size. Furthermore, the dependence of the raft domain size on the recycling rate, length, and raft area fraction were explored numerically, and the effects of membrane compartmentalization and immobile membrane proteins on raft formation were investigated. These results form the basis for an improved understanding of lipid raft formation and dynamics in plasma membranes, and highlight the need for a better understanding of the nonequilibrium cellular processes, which have the potential to regulate evolving microstructures in living cells.

ACKNOWLEDGMENTS

This work has been in part supported by NSF-DMR Grant No. DMR-0449184 and NSF-MRSEC Program Grant No. DMR-0213706 at Princeton University.

APPENDIX A: DERIVATION OF THE RECYCLING RATE *H*

In order to relate the recycling parameters to measurable physical quantities, we first derive the relation between the rate H and the probability p per unit time that a given lipid changes its type due to recycling. To this end, consider a system with two different lipid species which correspond to the raft and nonraft phases in this paper. Local variable $X_i(t)=-1$ (1) signifies that at location i lipid type one (two) is present at time t. Let N_{lipid} denote the total number of lipid molecules. $i=1,\ldots,N_{lipid}$.

After an infinitesimal time interval Δt, the probability that $X_i(t+\Delta t)=-X_i(t)$ is $p\Delta t$, and the probability that $X_i(t+\Delta t)=X_i(t)$ is $1-p\Delta t$. Here $p\Delta t$ is the probability that after time Δt at each location the lipid type has changed due to recycling. Now, $X(\Delta t)=\Sigma_{i=1}^{N_{lipid}}X_i(\Delta t)/N_{lipid}$, and $\langle X(\Delta t)\rangle$ and $\langle X^2(\Delta t)\rangle$ at time Δt, where $\langle\ldots\rangle$ denotes the average over all noise realizations, are given by

$$\langle X(\Delta t)\rangle = \sum_{i=1}^{N_{lipid}} \{X_i(0)(1-p\Delta t) + [-X_i(0)]p\Delta t\}/N_{lipid}$$
$$= X(0)(1-2p\Delta t), \tag{A1}$$

and

$$\langle X^2(\Delta t)\rangle = \left\langle \sum_{i=1}^{N_{lipid}} [X_i^2(\Delta t)]/N_{lipid}^2 \right\rangle + \left\langle \sum_{i=1}^{N_{lipid}} \sum_{j=1,j\neq i}^{N_{lipid}} X_i(\Delta t)X_j(\Delta t)/N_{lipid}^2 \right\rangle$$
$$= 1/N_{lipid} + [X^2(0) - 1/N_{lipid}](1-2p\Delta t)^2,$$
$$= 4p\Delta t(1-p\Delta t)/N_{lipid} + X^2(0)(1-2p\Delta t)^2. \tag{A2}$$

Thus,

$$\langle X^2(\Delta t)\rangle - \langle X(\Delta t)\rangle^2 = 4p\Delta t(1-p\Delta t)/N_{lipid}, \quad \text{(A3)}$$

which can be expanded to leading order in Δt as

$$\langle X^2(\Delta t)\rangle - \langle X(\Delta t)\rangle^2 = 4p\Delta t/N_{lipid}. \quad \text{(A4)}$$

From the continuum point of view, on the other hand, we can also calculate the fluctuation over the entire c field in the area $A=\int d\mathbf{r}$ in the same time interval with $\ell\to\infty$. To this end, we will only consider the effect of the recycling term, and write the change in the local composition as

$$c(\mathbf{r},\Delta t) = c(\mathbf{r},0) + \int_0^{\Delta t} dt'\,\eta(\mathbf{r},t'). \quad \text{(A5)}$$

Now, define the spatially averaged composition over the area as $\bar{C}\equiv A^{-1}\int d\mathbf{r}c(\mathbf{r},t)$. Thus,

$$\bar{C}(\Delta t) = \bar{C}(0) + A^{-1}\int d\mathbf{r}\int_0^{\Delta t} dt'\,\eta(\mathbf{r},t'). \quad \text{(A6)}$$

It is straightforward to show that

$$\langle \bar{C}(\Delta t)\rangle = \bar{C}(0), \quad \text{(A7)}$$

and

$$\langle \bar{C}^2(\Delta t)\rangle - \langle \bar{C}(\Delta t)\rangle^2 = A^{-2}\int d\mathbf{r}\int d\mathbf{r}'\int_0^{\Delta t} dt'\int_0^{\Delta t} dt''\langle \eta(\mathbf{r},t')\,\eta(\mathbf{r}',t'')\rangle. \quad \text{(A8)}$$

Finally, by employing the recycling noise correlator $\langle \eta(\mathbf{r},t')\,\eta(\mathbf{r}',t'')\rangle = \bar{H}^2\delta(\mathbf{r}-\mathbf{r})\,\delta(t'-t'')$, appropriate for $\ell\to\infty$, we obtain,

$$\langle \bar{C}^2(\Delta t)\rangle - \langle \bar{C}(\Delta t)\rangle^2 = \frac{\bar{H}^2\Delta t}{A}. \quad \text{(A9)}$$

Here, $\bar{H}$ denotes the dimensional recycling rate. Now, from dimensional analysis it can be derived that $H^2 = \bar{H}^2\tau v/(u\omega^2) = \bar{H}^2T^2/[3D(T_c-T)^2]$. Therefore the fluctuation as calculated from the continuum model becomes

$$\langle \bar{C}^2(\Delta t)\rangle - \langle \bar{C}(\Delta t)\rangle^2 = \frac{3D(T_c-T)^2H^2\Delta t}{AT^2}. \quad \text{(A10)}$$

The fluctuations in Eqs. (A4) and (A10) should be equal, and therefore $4p/N_{lipid} = 3H^2D(T_c-T)^2/AT^2$, which leads to,

$$p = 3H^2D(T_c-T)^2/(4A_{lipid}T_c^2), \quad \text{(A11)}$$

as $T\to T_c$, where A_{lipid} denotes the area per lipid.

APPENDIX B: DERIVATION OF THE CRITICAL $g(\mathbf{r})$

Without loss of generality, we will only consider the case $g(\mathbf{r})=g_0<0$ along the compartment boundaries. Compare the following two systems: (1) A single macroscopic domain of the $c=-1$ phase surrounded by the $c=1$ phase. The area fraction of the $c=-1$ domain is ϕ. The free energy per area of this system is

$$F_1 = f_{-1}\phi + f_1(1-\phi) + L_1\gamma/L^2 + A_g g_0(1-2\phi) \quad \text{(B1)}$$

where $f_{-1}(f_1)$ denotes the free energy per area of $c=-1$ $(+1)$ phase, L_1 is the interface length, L is the system size, and A_g is the area fraction of the compartment boundary region. When $L\to\infty$, $L_1\propto L$ and $L_1/L^2\to 0$ at fixed area fraction, and thus,

$$\lim_{L\to\infty} F_1 = f_{-1}\phi + f_1(1-\phi) + A_g g_0(1-2\phi). \quad \text{(B2)}$$

(2) A circular domain of the $c=-1$ phase surrounded by the $c=1$ phase resides in each square compartment of linear dimension L_c and boundary width a. The $c=1$ phase covers the region where $g(\mathbf{r})<0$. The free energy per area of this system is given by

$$F_2 = f_{-1}\phi + f_1(1-\phi) + L_2\gamma/L_c^2 + A_g g_0, \quad \text{(B3)}$$

where L_2 denotes the total interface length in each compartment. Now, the difference in the free energy densities between these two systems is

$$\Delta F = F_2 - F_1 = L_2\gamma/L_c^2 + 2A_g g_0\phi. \quad \text{(B4)}$$

Critical interaction strength g_0^* is thus obtained when $\Delta F=0$, implying

$$g_0^* = -\frac{L_2\gamma}{2A_gL_c^2} \approx -\frac{2\gamma\sqrt{\pi\phi}}{4aL_c^2}, \quad \text{(B5)}$$

where we have assumed in the last term that $a/L_c \ll 1$.

[1] S. J. Singer and G. L. Nicolson, Science **175**, 720 (1972).
[2] K. Jacobson, E. D. Sheets, and R. Simson, Science **268**, 1441 (1995).
[3] W. Rodgers and M. Glaser, Proc. Natl. Acad. Sci. U.S.A. **88**, 1364 (1991).
[4] A. Kusumi, Y. Sako, and M. Yamamoto, Biophys. J. **65**, 2021 (1993).
[5] R. Welti and M. Glaser, Chem. Phys. Lipids **73**, 121 (1994).
[6] D. A. Brown and E. London, J. Membr. Biol. **164**, 103 (1998).
[7] K. Simons and E. Ikonen, Nature (London) **387**, 569 (1997).
[8] D. A. Brown and E. London, Annu. Rev. Cell Dev. Biol. **14**, 111 (1998).
[9] K. Simons and D. Toomre, Nature Rev. Mol. Cell Biol. **1**, 31 (2000).
[10] M. Dykstra, A. Cherukuri, S. J. T. H. W. Sohn, and S. K. Pierce, Annu. Rev. Immunol. **21**, 457 (2003).
[11] E. Ikonen, Curr. Opin. Cell Biol. **13**, 470 (2001).
[12] C. Salaün, D. J. James, and L. H. Chamberlain, Traffic (Oxford, U.K.) **5**, 255 (2004).
[13] M. F. Hanzal-Bayer and J. F. Hancock, FEBS Lett. **581**, 2098

(2007).
[14] M. Bagnat, S. Keränen, A. Shevchenko, and K. Simons, Proc. Natl. Acad. Sci. U.S.A. **97**, 3254 (2000).
[15] D. H. Nguyen and J. E. K. Hildreth, J. Virol. **74**, 3264 (2000).
[16] S. M. Campbell, S. M. Crowe, and J. Mak, J. Clin. Virol. **22**, 217 (2001).
[17] N. Chazal and D. Gerlier, Microbiol. Mol. Biol. Rev. **67**, 226 (2003).
[18] B. C. Lagerholm, G. E. Weinreb, K. Jacobson, and N. L. Thompson, Annu. Rev. Phys. Chem. **56**, 309 (2005).
[19] T. Harder, P. Scheiffele, P. Verkade, and K. Simons, J. Cell Biol. **141**, 929 (1998).
[20] E. D. Sheets, G. M. Lee, R. Simson, and K. Jacobson, Biochem. **36**, 12449 (1997).
[21] R. Varma and S. Mayor, Nature (London) **394**, 798 (1998).
[22] J. Hwang, L. A. Gheber, L. Margolis, and M. Edidin, Biophys. J. **74**, 2184 (1998).
[23] G. J. Schütz, G. Kada, V. P. Pastushenko, and H. Schindler, EMBO J. **19**, 892 (2000).
[24] A. Pralle, P. Keller, E. L. Florin, K. Simons, and J. K. H. Horber, J. Cell Biol. **148**, 997 (2000).
[25] P.-F. Lenne, L. Wawrezinieck, F. Conchonaud, O. Wurta, A. Boned, X.-J. Gao, H. Rigneault, H.-T. He, and D. Marguet, EMBO J. **25**, 3245 (2006).
[26] K. Gaus, E. Gratton, E. P. W. Kable, A. S. Jones, I. Gelissen, L. Kritharides, and W. Jessup, Proc. Natl. Acad. Sci. U.S.A. **100**, 15554 (2003).
[27] C. Eggeling *et al.*, Nature (London) **457**, 1159 (2009).
[28] T. Friedrichson and T. V. Kurzhalia, Nature (London) **394**, 802 (1998).
[29] B. F. Lillemeier, J. R. Pfeiffer, Z. Surviladze, B. S. Wilson, and M. M. Davis, Proc. Natl. Acad. Sci. U.S.A. **103**, 18992 (2006).
[30] S. L. Veatch and S. L. Keller, Phys. Rev. Lett. **89**, 268101 (2002).
[31] M. B. Forstner, D. S. Martin, A. M. Navar, and J. A. Käs, Langmuir **19**, 4876 (2003).
[32] H. A. Rinia, M. M. E. Snel, J. P. J. M. van der Eerden, and B. de Kruijff, FEBS Lett. **501**, 92 (2001).
[33] L. A. Bagatolli and E. Gratton, J. Fluoresc. **11**, 141 (2001).
[34] S. L. Veatch and S. L. Keller, Biophys. J. **85**, 3074 (2003).
[35] S. L. Veatch, I. V. Polozov, K. Gawrisch, and S. L. Keller, Biophys. J. **86**, 2910 (2004).
[36] J. M. Besterman and R. B. Low, Biochem. J. **210**, 1 (1983).
[37] C. R. McMaster, Biochem. Cell Biol. **79**, 681 (2001).
[38] M. Brumen, R. Heinrich, A. Herrmann, and P. Müller, Eur. Biophys. J. **22**, 213 (1993).
[39] S. Frickenhaus and R. Heinrich, Biophys. J. **76**, 1293 (1999).
[40] T. Pomorski, S. Hrafnsdóttir, P. E. Devaux, and G. van Meer, Semin Cell Dev. Biol. **12**, 139 (2001).
[41] P. F. Devaux, I. López-Montero, and S. Bryde, Chem. Phys. Lipids **141**, 119 (2006).
[42] M. S. Bretscher, Nature New Biol. **236**, 11 (1972).
[43] A. Yethiraj and J. C. Weisshaar, Biophys. J. **93**, 3113 (2007).
[44] P. Guilmin and L. Turban, J. Phys. C **13**, 4077 (1980).
[45] M. F. Thorpe and D. Beeman, Phys. Rev. B **14**, 188 (1976).
[46] A. Pekalski and T. Oguchi, Prog. Theor. Phys. **54**, 1021 (1975).
[47] L. Foret, Europhys. Lett. **71**, 508 (2005).
[48] F. Liu and N. Goldenfeld, Phys. Rev. A **39**, 4805 (1989).
[49] S. L. Veatch, P. Cicuta, P. Sengupta, A. Honerkamp-Smith, D. Holowka, and B. Baird, ACS Chem. Biol. **3**, 287 (2008).
[50] M. S. Turner, P. Sens, and N. D. Socci, Phys. Rev. Lett. **95**, 168301 (2005).
[51] L. A. Gheber and M. Edidin, Biophys. J. **77**, 3163 (1999).
[52] J. Fan, M. Sammalkorpi, and M. Haataja, Phys. Rev. Lett. **100**, 178102 (2008).
[53] J. Gómez, F. Sagués, and R. Reigada, Phys. Rev. E **77**, 021907 (2008).
[54] J. Gómez, F. Sagués, and R. Reigada, Phys. Rev. E **80**, 011920 (2009).
[55] J. Fan, M. Sammalkorpi, and M. Haataja, FEBS Lett. (to be published).
[56] M. Müller, K. Katsov, and M. Schick, Phys. Rep. **434**, 113 (2006).
[57] S. A. Pandit, S. Vasudevan, S. W. Chiu, R. J. Mashl, E. Jakobsson, and H. L. Scott, Biophys. J. **87**, 1092 (2004).
[58] P. S. Niemelä, S. Ollila, M. T. Hyvönen, M. Karttunen, and I. Vattulainen, PLOS Comput. Biol. **3**, 304 (2007).
[59] H. J. Risselada and S. J. Marrink, Proc. Natl. Acad. Sci. U.S.A. **105**, 17367 (2008).
[60] R. Faller and S.-J. Marrink, Langmuir **20**, 7686 (2004).
[61] M. Laradji and P. B. S. Kumar, J. Chem. Phys. **123**, 224902 (2005).
[62] G. Illya, R. Lipowsky, and J. C. Shillcock, J. Chem. Phys. **125**, 114710 (2006).
[63] S. Yamamoto and S. Hyodo, J. Chem. Phys. **118**, 7937 (2003).
[64] J. C. Shillcock and R. Lipowsky, J. Chem. Phys. **117**, 5048 (2002).
[65] M. Venturoli, M. M. Sperotto, M. Kranenburg, and B. Smit, Phys. Rep. **437**, 1 (2006).
[66] G. S. Ayton and G. A. Voth, Biophys. J. **87**, 3299 (2004).
[67] J. L. McWhirter, G. Ayton, and G. A. Voth, Biophys. J. **87**, 3242 (2004).
[68] G. S. Ayton, J. L. McWhirter, P. McMurtry, and G. A. Voth, Biophys. J. **88**, 3855 (2005).
[69] P. B. Sunil Kumar, G. Gompper, and R. Lipowsky, Phys. Rev. E **60**, 4610 (1999).
[70] Y. Jiang, T. Lookman, and A. Saxena, Phys. Rev. E **61**, R57 (2000).
[71] C. M. Funkhouser, F. J. Solis, and K. Thornton, Phys. Rev. E **76**, 011912 (2007).
[72] A. Radhakrishnan and H. McConnell, Proc. Natl. Acad. Sci. U.S.A. **102**, 12662 (2005).
[73] J. W. Cahn and J. E. Hilliard, J. Chem. Phys. **28**, 258 (1958).
[74] P. C. Hohenberg and B. I. Halperin, Rev. Mod. Phys. **49**, 435 (1977).
[75] A. J. Bray, Adv. Phys. **51**, 481 (2002).
[76] H. E. Cook, Acta Metall. **18**, 297 (1970).
[77] T. M. Rogers, K. R. Elder, and R. C. Desai, Phys. Rev. B **37**, 9638 (1988).
[78] G. Grinstein, D. H. Lee, and S. Sachdev, Phys. Rev. Lett. **64**, 1927 (1990).
[79] M. Saxton and K. Jacobson, Annu. Rev. Biophys. Biomol. Struct. **26**, 373 (1997).
[80] K. Jacobson, O. G. Mouritsen, and R. G. W. Anderson, Nat. Cell Biol. **9**, 7 (2007).
[81] J. Fan, M. Sammalkorpi, and M. Haataja, (unpublished).
[82] J. Valdez-Taubas and H. R. B. Pelham, Curr. Biol. **13**, 1636 (2003).
[83] K. E. Mostov, M. Verges, and Y. Altschuler, Curr. Opin. Cell

Biol. **12**, 483 (2000).
[84] T. A. Slimane, G. Trugnan, S. C. D. van IJzendoorn, and D. Hoekstra, Mol. Biol. Cell **14**, 611 (2003).
[85] A. Kusumi, I. Koyama-Honda, and K. Suzuki, Traffic (Oxford, U.K.) **5**, 213 (2004).
[86] Y. M. Umemura, M. Vrljic, S. Y. Nishimura, T. K. Fujiwana, K. G. N. Suzuki, and A. Kusumi, Biophys. J. **95**, 435 (2008).
[87] M. de Berg, M. van Kreveld, M. Overmans, and O. Schwarzkopf, *Computational Geometry: Algorithms and Applications* (Springer, New York, 2000).
[88] M. Edidin, Annu. Rev. Biophys. Biomol. Struct. **32**, 257 (2003).
[89] M. M. Hao and F. R. Maxfield, J. Biol. Chem. **275**, 15279 (2000).
[90] B. J. Nichols, A. K. Kenworthy, R. S. Polishchuk, R. Lodge, T. H. Roberts, K. Hirscberg, R. D. Phair, and J. Lippincott-Schwatrz, J. Cell Biol. **153**, 529 (2001).
[91] M. A. Kol, A. van Dalen, A. I. P. M. de Kroon, and B. de Kruijff, J. Biol. Chem. **278**, 24586 (2003).
[92] Y. Li and W. A. Prinz, J. Biol. Chem. **279**, 45226 (2004).
[93] J. C. M. Holthuis and T. P. Levine, Nat. Rev. Mol. Cell Biol. **6**, 209 (2005).
[94] Q. Tang and M. Edidin, Biophys. J. **81**, 196 (2001).
[95] B. Winckler, P. Forscher, and I. Mellman, Nature (London) **397**, 698 (1999).
[96] T. Fujiwara, K. Ritchie, H. Murakoshi, K. Jacobson, and A. Kusumi, J. Cell Biol. **157**, 1071 (2002).
[97] C. Nakada, K. Ritchie, Y. Oba, M. Nakamura, Y. Hotta, R. Iino, R. S. Kasai, K. Yamaguchi, T. Fujiwara, and A. Kusumi, Nat. Cell Biol. **5**, 626 (2003).
[98] K. Schmidt and B. J. Nichols, Curr. Biol. **14**, 1002 (2004).
[99] A. D. Douglass and R. D. Vale, Cell **121**, 937 (2005).
[100] S. J. Plowman, C. Muncke, R. G. Parton, and J. F. Hancock, Proc. Natl. Acad. Sci. U.S.A. **102**, 15500 (2005).
[101] K. A. Melkonian, A. G. Ostermeyer, J. Z. Chen, M. G. Roth, and D. A. Brown, J. Biol. Chem. **274**, 3910 (1999).
[102] S. Moffett, D. A. Brown, and M. E. Linder, J. Biol. Chem. **275**, 2191 (2000).
[103] R. G. W. Anderson and K. Jacobson, Science **296**, 1821 (2002).
[104] L. Pike, J. Lipid Res. **44**, 655 (2003).
[105] K. Lim and J. Yin, Biotechnol. Bioeng. **90**, 694 (2005).
[106] J. A. Allen, R. A. Halverson-Tamboli, and M. M. Rasenick, Nat. Rev. Neurosci. **8**, 128 (2007).
[107] J. F. Hancock, Nat. Rev. Mol. Cell Biol. **7**, 456 (2006).
[108] J. L. Thomas, D. Holowka, B. Baird, and W. W. Webb, J. Cell Biol. **125**, 795 (1994).
[109] D. A. Brown and E. London, Biochem. Biophys. Res. Commun. **240**, 1 (1997).